Volume : 4 | Issue : 10 | October 2015 • ISSN No 2277 - 8179

Research Paper

Composition Dependent Structural and Optical Properties of Mn Doped ZnO Nanoparticles

Physics

KEYWORDS : Nanoparticle; Semiconductor; Transmittance; Optoelectronics; Wavelength; Quantum

S. Kanchana	PG & Research Department of Physics,Urumu Dhanalaksmi College, Tiruchirapalli-620 019, Tamilnadu India.
K. Pushpanathan	PG & Research Department of Physics, Government Arts College, Karur- 639 005. Tamilnadu ,India.
Suhashini Ernest	PG & Research Department of Physics,Urumu Dhanalaksmi College, Tiruchirapalli-620 019, Tamilnadu India.

ABSTRACT

This article deals with the preparation and characterization of manganese doped zinc oxide nanopowder. Prepared samples were examined by means of x-ray diffractometer, scanning electron microscope, ultraviolet-visible spectrometer, fourier transform infrared spectrometer, and photoluminescence spectrometer to study effect of manganese doping on crystalline size, microstructure, optical properties and energy gap. X-ray diffraction study confirmed the incorporation of manganese ion in place of zinc ion without disturbing the basic hexagonal wurtzite structure of zinc oxide nanocrystal. The average grain size was calculated from the X-ray line broadening and it was found increase for manganese doped samples as compared to undoped zinc oxide. Scanning electron microscope image also confirmed the existence of nano size particle. It is found that the energy gap of the doped zinc oxide decreases with increase of manganese content. Study on photoluminescence properties confirmed the substitution of manganese in zinc oxide through the blue emission in 450-490 nm range.

1. Introduction

Zinc Oxide (ZnO) is known from 1935, but it receives great attention for the past two decades only, due to its distinguished performance in smart devices in the form of nanoparticles [1-7]. Compared to other wide energy gap metal-oxide nonmaterial, ZnO possesses a very large exciton binding energy (60 eV) at room temperature and a wide energy gap of 3.37 eV. It has a stable hexagonal structure (wurtzite structure) at room temperature with lattice constant a = 3.251 and c = 5.210 [8] and composed of a number of alternating planes with tetrahedrally-coordinated O^{2-} and Zn^{2+} ions stacked alternatively along the c-axis. Basically, it is an II-VI group *n type* semiconductor, having a very good optical transparency for visible spectrum, even at higher carrier concentration, making ZnO a promising material in transparent electronics, optoelectronics, integrated sensors, Ultra-Violet (UV) light emitters [9], UV nanolasers [10], UV Photodetectors, photodiodes, high flame detectors [11], nanosensors for various gases, blue color light emitting phosphors [12,13], varistors, solar cells. It is well known from the pervious report that ZnO nanoparticles have advanced optical properties than its bulk form, because of its quantum confinement effect. The electrical property and bandgap of ZnO is almost the same as that of Titanium Oxide (TiO_2), however ZnO is more efficient than TiO_2. As mentioned above, ZnO is very useful in solar energy conversion, due to wide energy gap it can't be used directly. In order to reduce the energy gap, it is being doped with the Transition Metals (TM) like Mn, Ni, Cu, Mg, Li, Al, Co, Cr, Fe, V and Ti [14-20]. Of these, Mn doping has attracted the rigorous interest in recent years.

Mn doped ZnO is commonly known as Diluted Magnetic Semiconductors (DMS) that show signs of both ferromagnetism and semiconducting properties [21]. Dietl et al [22] theoretically predicted that Mn doped ZnO would show ferromagnetic behavior with Curie temperature (T_c) above room temperature. Later on, Sharma et al [23], experimentally proved the room temperature ferromagnetism in bulk Mn doped ZnO. Henceforth, an important era started towards spintronic devices that use both charge and spin for reading and writing information. Origin of ferromagnetism in this material is still not clear, but for instance, Jayakumar [24] and his research group reported that the incorporation of Mn^{2+} ions into the ZnO lattice is the root cause of ferromagnetism. Contradictorily, some other research group believed that the secondary phases of magnetic clusters or their oxides might be responsible for the ferromagnetism in this system [25, 26].

Extensive literature survey revealed that the properties of Mn doped nanoparticles, like the band gap, optical absorbance and transmission, photoluminescence are influenced greatly by the quantum confinement effect. In addition, Mn has more than 10mol% thermal solubility in ZnO and the effective mass of electron is as large as ~0.3 times of free electron mass. Therefore, the amount of injected spins and carriers are large, thus making Mn doped ZnO ideal for spintronic devices. These interesting properties of Mn doped ZnO nanoparticles have increased the scope of research in this material for us.

A variety of methods have been adapted to synthesis Mn doped ZnO nanoparticles. Most of them are conventional high temperature solid state reaction method, in which, controlling the particle properties is complex, and also those are energy consuming and time consuming processes. On the other hand, Mn doped ZnO nanoparticles can be prepared on a large scale at low cost by simple solution based method, such as hydrothermal reaction, chemical precipitation, direct precipitation method and sol-gel synthesis. Among these techniques, direct precipitation method is a promising alternative synthesis method because of its easy procedure, easy control of particle size and property, low-cost processing, coating ability to even large size particle and low temperature process. Wide range of literature review infers that precipitation method is the main method of synthesis of Mn doped ZnO nanoparticles. The powder obtained from this method has uniform doping, smallest particle size with best optical and photocatalytic activity, compared to the powders obtained from the above mentioned methods [27] Due to these reasons, precipitation method has been adopted for the present work.

The main goal of this work is to evaluate the effect of Mn doping on microstructure, crystal structure, optical properties and energy gap of ZnO nanoparticles prepared by precipitation method. Previous experimental reports shows that room temperature ferromagnetism is possible in Mn doped ZnO nanoparticles for a very dilute concentration of Mn of the order of 2% [22]. This has been further confirmed by Rajkumar et al [28], in their work they found ferromagnetism up to 3at % (1.3 at% in EDS analysis) of Mn. In similar manner, Ullah and J.Dutta [29] have reported

1% of Mn is the optimum dopant concentration to achieve maximum optical absorption. Hence, 1% and 2% Mn concentration has been selected for doping for the present study. Even though synthesis and characterization of Mn doped ZnO nanoparticle is the routine nature, the most significant finding of the present work is that the undoped ZnO nanoparticles may have the energy gap around 3.82 eV and 1% Mn doping reduces greatly the energy gap of ZnO by 0.43 eV.

2. Materials and Methods

Undoped and Mn doped ZnO nanoparticles were synthesized by chemical precipitation method from the appropriate ratio of zinc acetate and manganese acetate. High purity chemicals of zinc acetate di-hydrate ($Zn(CH_3COOH)_2 \cdot 2H_2O$ 99.5%, Merck), manganese acetate $Mn(CH_3COO)_2 \cdot 4H_2O$ 99.5%, Merck) tetra hydrate and sodium hydroxide (NaOH, Merck) were used without further purification. Briefly, for undoped ZnO nanoparticles, 4 gms of zinc acetate dihydrate was dissolved in a 200 ml of double distilled water in a conical flask and magnetically stirred for 15 minutes to get the uniformly concentrated zinc acetate solution. Then, 12 gms of sodium hydroxide pellets were dropped slowly into the zinc acetate solution under constant stir of 150 rpm. The solution turned into a milky white and the precipitation formed in the solution was separated by filtering then washed many times with double distilled water and ethanol. The ZnO nanoparticles obtained so was dried at 80 ˚C for 4 hours in a hot oven so as to remove water molecules from the product.

Mn doped ZnO samples were synthesized at two different Mn concentrations of 1 at% and 2 at% by adding appropriate amount of manganese acetate tetrahydrate to the zinc acetate solution, using the same procedure mentioned above. Hereafter, the undoped ZnO, 1% and 2% Mn doped samples are referred as Undoped, Mn-1% and Mn-2%, respectively. Polyethylene glycol (MW: 400) was used as capping agent.

Crystal structure identification was performed using an X-Ray Diffractometer (Philips Analytical Model No.-PW1830) equipped with Ni filtered CuKα radiation (α = 1.54187 Å) for 2θ = 30 - 80˚, with scanning rate of "5˚" min^{-1}" operated at 40 kV/30 mA. Surface morphology and microstructure of the particles was studied by using JEOL Scanning Electron Microscope (JSM-6390: Japan) operated at 20kV/ 20mA. Chemical composition of the synthesized ZnO nanoparticles was examined by Energy-Dispersive X-ray Spectrometer (EDS: INCAPentaFET-x3, Oxford Instruments, UK). To identify the functional groups and to confirm the presence Mn^{2+} ions, the samples were examined with Fourier Transform Infrared Spectrometer (FTIR; RX1 PERKINELMER: USA) at a resolution of 2 cm^{-1} and sample scan time as well as background scan time of 32 scans for all the samples. The measurements were carried out in the region 400–4000 cm^{-1} using KBr as the beam splitter. In addition to this, optical properties of the samples were also studied by using Lambda **35** (PERKINELMER: USA) UV-Vis spectrophotometer in the range from 190–1100 nm at room temperature. For this study, the powder samples were dispersed in deionized water and mixed well. Photoluminescence (PL) measurement was carried out by means PL spectrometer (Kimon, SPEC-14031K, Japan) with a He-Cd laser line of 325 nm as the excitation source.

3. Results and Discussion

3.1 Structural analysis

X-Ray Diffraction (XRD) pattern of the undoped ZnO and Mn doped ZnO nanopowders are displayed in Figure 1. Prominent peaks at 31.6, 34.3, 36.2, 47.4, 56.5, 62.7, 66.2, 67.8, 69.0, 72.4 and 76.8 corresponding to (100), (002), (101), (102), (110), (103), (200), (112) , (201), (004) and (202) planes, confirms that all the three samples possesses wurtzite structure of ZnO (hexagonal phase). Lattice of the sample is all similar to the values available in the JCPDS data card 80-0075 (space group $P6_3mc$)). This reveals that without affecting the wurtzite structure, the Mn atoms are doped into the ZnO structure. Furthermore, intensity of the diffraction peaks determines the quality of the nano crystal. We recorded the maximum intensity of 400 cps, 3000 cps and 3750 cps (not shown in the figure) for undoped, Mn-1% and Mn-2% samples, respectively. This increase in intensity of the diffraction peaks with the increase on the Mn content shows that the quality of the nanoparticles increases upon Mn doping. For all the samples, (101) peak has the highest intensity. With reference to this peak, average grain size'*d*' of the prepared samples has been calculated According to the Debye – Scherrer formula [30], shown in Eqn (1).

$$d = \frac{0.89\,\lambda}{\beta\,\cos\theta} \quad \text{---------- (1)}$$

Where λ is the wavelength of CuK_α radiations (0.154 nm), β is the Full Width at Half- Maximum (FWHM) of the peaks and θ is the angle obtained from 2θ value corresponding to maximum intensity peak in XRD pattern. The calculated average grain size to be 19.8 nm for undoped ZnO, it increases to 43 nm on 1% Mn doping and it again decreases to 29.1 nm on further doping of 2%. As seen, doping increases/decreases the grain size and this type of increase/decrease in grain size has already been reported [31, 32]. The lattice constant of the samples have been found, according to the following Eqn (2) and recorded in Table 1.

$$\frac{1}{d^2} = \frac{4}{3}\left\{\frac{h^2+hk+k^2}{a^2}\right\} + \frac{l^2}{c^2} \quad \text{---------- (2)}$$

It can be seen that the lattice parameter 'a' and 'c' of sample Mn-1% is comparatively larger than the undoped ZnO and gets decreased slightly for Mn-2% sample. The absence of any excess peak concludes that ZnO/ Mn doped ZnO samples prepared by precipitation method under room temperature are highly pure and single crystalline.

With the help of position of (101) peak, substitution of Mn^{2+} or impurity phase like Mn^{3+} or Mn^{4+} in place of Zn^{2+} can be easily detected. With respect to undoped sample, the lattice constant of the Mn-1% sample is increased. It is due to the substitution of Mn^{2+} in Zn^{2+}sites. Ionic radius of Mn^{2+} is (0.66 Å) is larger than the ionic radius of Zn^{2+} (0.60 Å). Due to larger size of Mn^{2+} ions, the lattice parameter gets increased. Therefore, increase in lattice constant confirms the substitution of Mn^{2+} without affecting the wurtzite structure of the ZnO. In the case of Mn-2% sample, the peak (101) shifts towards the higher angle. Consequently, lattice constant gets decreased. It is suspected that it may be due to the substitution of very small amount of Mn^{3+} and Mn^{4+} in Zn^{2+}sites, instead of Mn^{2+}. As the ionic radius of the Mn^{3+} (0.58 Å) and Mn^{4+} (0.53 Å) is smaller than Mn^{2+}, the lattice constant decreased for 2% Mn doping. The increase and decrease in lattice constant and the slight shift of XRD peaks towards higher/ lower angle confirms that Mn is really doped into ZnO. Others have also observed similar trend of deformation (increase/ decrease) in lattice constant as a result of Mn doping in ZnO [33,34]. Table 1, summarizes the average grain size, lattice parameter, unit cell volume of the undoped and Mn doped ZnO samples. The result presented here suggests that the precipitation method at room temperature is suitable method to prepare the single phase and single crystalline ZnO nanoparticles. Moreover, the XRD result implies that the solubility of Mn increases in ZnO nanostructures. Figure 2(a-c) depicts the variation of grain size, lattice constant, c/a ratio and unit cell volume of the synthesized samples versus Mn content.

The band gap of nanoparticles in terms of radius has been determined from the effective mass model expression [35], as given below

$$E_g^{nano} = E_g^{bulk} + \frac{h^2}{8er^2}\left[\frac{1}{m_e^*} + \frac{1}{m_h^*}\right] - \frac{1.8e^2}{4\pi\epsilon\varepsilon_0 r}$$

---------- (3)

Where, E_g^{bulk} is the energy gap of bulk ZnO (3.37 eV) , r is radius of the nanoparticles calculated from <101> plane of XRD pattern , m_e^* is the effective mass of the electrons (0.24 m_o), m_h^* is the effective mass of holes (0.45 m_o), m_o is the rest mass of the electron (9.110×10^{-31} kg), ε is the relative permittivity (8.66), ε_0 is the permittivity of free space (8.854×10^{-12} F m^{-1}) , h is Planck's constant (6.626×10^{-34} Js), and e is the charge of an electron (1.602×10^{-19} C). Using the above equation, calculated band gap of the undoped sample is 3.43 eV. Then it reduces to 3.40 eV for Mn-1% and again increases to 3.42 eV for Mn-2% sample.

3.2. Compositional analysis

The EDX spectra of the samples used for the present study are displayed here. The spectrum shown in Figure 3(a) consists of Zn and O where as the Figure 3(b) and 3(c) confirms the presence of manganese in the ZnO particles. The atomic ratio (x) of Mn to Zn determined from the relation x = Mn/([Zn +Mn]) to be x = 0.30 % for 1% and 0.63% for 2% doping. EDX analysis gives how much amount of Mn atom has really entered into the ZnO nanoparticles. We actually doped 1% and 2% Mn. But the EDS analysis shows that only 0.3% and 0.6% of Mn atoms has entered into the ZnO. Remaining Mn atoms should have been washed away (or) clusters should have been formed. But, we haven't recorded any unusual changes, accountable for clusters; it is assumed that rest of the Mn atom has been removed on washing. Both atomic percentage (at%) and weight percentage (wt%) shown in Table 2 proves that the ratio of Mn dopant in the samples are ~1:2. Therefore, composition analysis confirms the incorporation of Mn element in the samples and also, it is clear that the amount of doping is exclusively based on the increase of Mn content in the solution. Others have also reported similar EDAX spectrum, as a result of Mn impurity doping with ZnO nanoparticles [36]

3.3. Microstructure analysis

Surface morphology of the undoped and Mn doped ZnO samples are shown in the Figures 4(a-c). The surface feature of undoped ZnO nanoparticles Fig.4(a) reveals the presence of sphere like grains. By reason of agglomeration, the boundaries can't be seen in distinguished manner. It is good-looking to note that the particles regular, and are uniform size distribution of about 18-24 nm. Furthermore, the effect of Mn doping on microstructure of the ZnO nanoparticles can be seen clearly in the respective figures. It is exciting to note that, 1% of Mn doping changed the microstructure from regular sphere shape to flower-like structure with some needle-like structure (refer Fig. 4(b)). However, the grain boundaries are clear in this case also. Obviously, in 2% Mn doped sample (Fig. 4(c)), the flower like structure is disappeared and the entire sample consists of needle like structure. The average diameter of the nano-needle is about 34-40 nm for Mn-1% and 23-38 nm for for Mn-2% sample. This is in agreement with the average grain size obtained from XRD. It should be noted that X-ray diffraction method is an indirect method, but the scanning electron microscopy is a direct method for the determination of particle size. So, SEM is reliable to determine the grain size. It may be noted that microstructure of Mn doped ZnO is sensitive to preparation method. Preparation by combustion method yields nanowires [37], direct precipitation method yields spherical, sol-gel method yields aggregated chain like form and the hydrothermal method may yield rod-like [38,39]. Therefore, from the SEM analysis, it is clear that the microstructure ZnO is responsive to Mn content. The observed spherical particles of undoped ZnO, flower like and rod-like structures of Mn doped samples presented here, confirms the earlier report [40].

3.4 Energy gap calculation from Tauc's Relation

The optical band gap of the prepared undoped and Mn doped samples has been calculated using the Tauc's relation [41]

$$(\alpha h\upsilon)^2 = A\,(h\upsilon - E_g) \qquad (5)$$

Where A is a constant, E_g is the energy of the photon involved in FTIR spectrum, α is the absorption coefficient, and E_g is the energy gap of the nanoparticle under investigation. Figure 5(a-c) depicts the optical band gap of the prepared samples. The energy gap E_g is estimated from the intercept of the linear portion of the curve on x-axis. Estimated band gap to be 3.82 eV for undoped (Fig.5(a)) and it decreases to 3.39 eV for 1% Mn doping, refer Fig.5(b). Referring to Fig. 5(c) further doping slightly increases the E_g again to 3.59 eV. The observed blue shift in energy gap is because of Mn doping in ZnO. The measurement shows that the E_g decreases/increases as the Mn content increases. Particle size and energy gap of the undoped and doped samples calculated in different method is shown in Table 3.

3.5 Photoluminescence spectrum

Photoluminescence spectrum, at room temperature has been recorded to analyze the effect of Mn content on the structural defects and the energy gap of ZnO nanoparticles. PL spectrum of undoped sample , shown in Figure 6(a), exhibits five emission lines such as; one in UV range (390 nm), one in violet range (~ 446 nm), one in blue range at (~ 488 nm), and two in green range at (~ 514 and 533 nm) ,which indicates that many oxygen vacancies exist in undoped sample. Of these, UV and Violet emissions are wide and the blue emission line is sharp and narrow. It is reported that the UV band emission originates from the exciton recombination corresponding to the Near Band Edge (NBE) [42]. Through exciton-exciton collision, this recombination occurs. The origin of the violet emission from the undoped ZnO is assumed to be the recombination from the defect centers such as O and Zn interstitials. It is reasonable to consider that this type of violet emission is rarely reported. The luminescent peak centered at 488 nm is assigned to the blue excitonic emission, corresponding to the band emission of 2.54 eV. Two sharp but less intense peaks around 514 nm (2.42 eV) and at 530 nm (2.35 eV) represents green emission, which is attributed to the single ionized oxygen vacancy in the ZnO should be produced at the time of sample preparation [43]

Comparing to undoped sample, it is attractive that in Mn doped samples UV and violet peaks are completely concealed and there is no trace of UV emission. At the same time, the blue and green emissions are obviously enhanced, as shown in Figure 6(b). The enhancement in blue and green emission results from the increment in oxygen vacancies, which are induced by Mn doping. From the photoluminescence study, it is clear that even low amount of Mn doping also severely suppress the luminescence power of undoped ZnO, which is in good agreement with the results reported in the literature [44]. Furthermore, it is noticeable that for 1% of Mn doping, blue emission peak around 487 nm is well sharp and the green emission line also single. But for 2% doping, blue emission line covers a range from 484-490 nm and in addition to the peak around ~519 nm, two more green emissions around ~533 nm, ~544 nm arises. This indicates that more number of oxygen vacancies are induced on Mn doping. This type of unusual photoluminescence property may be attributed to the unusual changes in the lattice parameter of the Mn doped sample reported here and we hope that this type of unusual photoluminescence property hasn't been published elsewhere to the best of our knowledge. Study on structural and photoluminescence properties of Mn doped ZnO nanoparticle shows that the shift in near band edge emission at 390 nm and blue emission in 450-490 nm range, confirmed the substitution on Mn in ZnO.

Volume : 4 | Issue : 10 | October 2015 • ISSN No 2277 - 8179

3.6 FTIR Spectrum

FTIR spectrum of the Mn doped and undoped ZnO nanopowders is shown in Figure 7, in which the broad absorption peak around 3,426 cm^{-1} shows the presence of O–H stretching of water in the undoped ZnO nanocrystals. The same peak is shifted to lower wavenumber of around 3,275 cm^{-1} for 1% Mn doping and again shifted to higher wavenumber around 3,395 cm^{-1} for its 2% Mn counterparts [45]. Presence of this strong and broad band suggests that drying the sample at 80 °C for 4 hours is inadequate to completely remove the moisture from the sample. This observation infers that annealing is required to remove the entrapped water in the samples. The absorption peaks observed between 2538 cm^{-1} and 2274 cm^{-1} is because of the absorbance of CO_2 molecule from the atmospheric air. Likewise, absorption peaks observed at 1,573 and 1,495 cm^{-1} of undoped ZnO corresponds the asymmetric and symmetric stretching of the carboxyl group (C=O) and the same is shifted to 1603 cm^{-1} and 1611 cm^{-1} for 1% and 2% Mn doped samples, respectively. Presence of (COO^-) is represented by minor absorption at 1383 cm^{-1}, probably from the unreacted acetates. But we haven't seen any XRD peaks relevant to unreacted acetates. The deformation bands of C=O also has been recorded around 1000 cm^{-1}. C-C vibration has been noticed at 1040 cm^{-1} for undoped sample, and at 1145 cm^{-1} for Mn-1% sample. O-H symmetric bending has been recorded for all the three samples between 1224 and 1292 cm^{-1}. Wavenumber 914 cm^{-1} belongs to -CH_2 vibration, it can be seen only for undoped sample. FTIR peaks and their assignments are displayed in table 4.

The effect of doping level in FTIR spectra is clearly observed in the region 1707 – 603 cm^{-1}. The spectrum indicates that the Mn doping has some effect on C- O band (1383 cm^{-1}) and vibration bands of C-C (1040 and 1145 cm^{-1}). Furthermore, it is observed from the spectra that the doping of Mn^{2+} ion towards Zn^{2+} (1% and 2% Mn) resulted in the absence of C=O deformation band at 1,573 cm^{-1}, carboxylate group (COO-) at 1,495 cm^{-1}, and C- O band at 1383 cm^{-1}. In addition to this, one more week characteristic absorption band at 914 cm^{-1} too almost disappeared. This is the sign of substitution of Zn^{2+} ions by Mn^{2+} ions in the ZnO crystal. Zn–O stretching mode is clearly centered in undoped ZnO nanopowder at about 566 cm^{-1} and it is observed at 603 cm^{-1} for 1%Mn concentration. Further doping of 2%, Zn–O stretching mode is once again shifted to 586 cm^{-1}. The shift in vibration frequency from 566 to 603 cm^{-1} is suggestive of incorporation of Mn^{2+} in the octahedral and tetrahedral sites of wurtzite structure. This difference in frequency is caused by the difference in the bond length that occurs when Mn ion replaces the Zn ion. The additional peaks around 822 cm^{-1} confirm the replacement of certain percent of Zn^{2+} by Mn^{2+} and this correspond to Mn–O stretching frequency. Result of FTIR spectrum is concomitant with the XRD and UV-Vis spectra results.

4. Conclusion

Nanocrystals of undoped and Mn doped ZnO were successfully synthesized by using a chemical precipitation method. XRD analysis concludes that prepared samples contain the particles in the range of 19-43 nm and also it confirms that Mn ions are definitely doped in ZnO without affecting the basic hexagonal wurtzite structure. The EDS analysis also confirmed the Mn doping. From the band gap measurement, it is concluded that 1%Mn doping lowers the energy gap of ZnO nanoparticles by 0.43 eV. The SEM results also confirm the presence of nanometer size crystals in the sample. Moreover, SEM analysis concludes that the microstructure of ZnO is sensitive to Mn doping and the morphology is distorted from sphere to rod like structure. The main important finding of this work is that the undoped ZnO nanoparticle may have the energy gap of 3.82 eV. Finally it is concluded that chemical precipitation method is a suitable method for the preparation of small size Mn doped ZnO nanoparticles.

TABLE CAPTIONS

Table 1. Grain size, lattice parameter, unit cell volume and (c/a) ratio of prepared undoped / Mn doped ZnO nanoparticles

Sample	Position of (101) peak (2θ) deg	FWHM (2θ) deg	Grain size (nm)	Lattice parameter		(c/a) ratio	Unit cell volume $(A^0)^3$
				a (Å)	c (Å)		
Undoped ZnO	36.150	0.440	19.8	3.258	5.218	1.6014	46.9
Mn – 1%	36.113	0.300	43.0	3.264	5.226	1.6009	46.6
Mn – 2%	36.144	0.203	29.1	3.261	5.222	1.6016	46.7

Table 2. Result of elemental analysis of undoped / Mn doped ZnO nanoparticles

Elements	Composition in (wt %)			Composition in (at %)		
	Undoped	Mn -1%	Mn -2%	Undoped	Mn -1%	Mn -2%
Zn	68.83	79.14	83.02	37.82	48.50	55.31
O	27.70	20.45	16.19	62.18	51.20	44.06
Mn	-	0.42	0.79	-	0.30	0.63
Total	100	100	100	100	100	100

Table 3: Relation between particle size and energy gap of the doped and undoped samples calculated in different methods.

Sample	Particle Size (nm) calculated		Energy Gap (eV) calculated from	
	From XRD	From SEM	Equn (3)	Tauc's Equn
Undoped	19.8	18-24	3.43	3.82
Mn-1%	43.0	34-40	3.40	3.39
Mn-2%	29.1	23-38	3.42	3.59

Table 4: IR peaks and their assignments for prepared nanoparticles

Assignments	Wavenumber (cm^{-1})		
	Undoped	Mn-1%	Mn-2%
O–H stretching of water	3426	3275	3395
existence of CO_2	2538	2274	Absent
C- O band	1383	-	-
C=O band	1573	1603	1611
carboxylate group (COO-)	1,495	absent	absent
C- C vibration	1040	1145	-
-CH_2 Vibration	914	absent	absent
O-H symmetric bending	1224	1263	1292
Stretching vibration of Zn-O	566	603	586
Mn–O stretching frequency	-	822	832

FIGURE CAPTIONS

Figure 1. X-ray diffraction pattern of undoped and Mn doped samples recorded at room temperature.

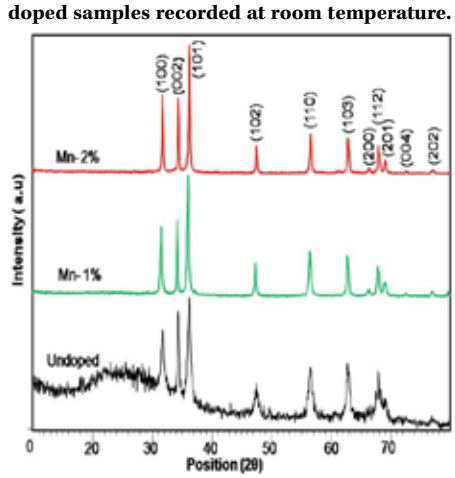


Figure 2 (a). Mn content vs grain size of the prepared samples.

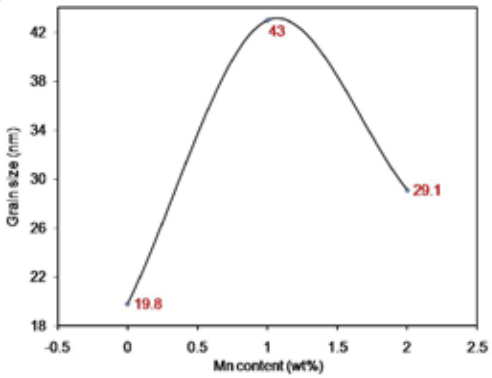


Figure 2 (b). Mn content vs lattice parameter of the synthesized nanopowders.

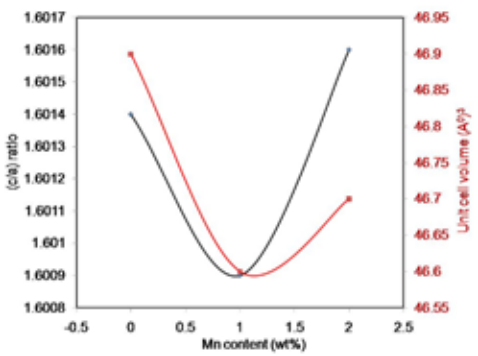


Figure 2 (c). Mn content vs unit cell volume and (c/a) ratio of the synthesized nanopowders.

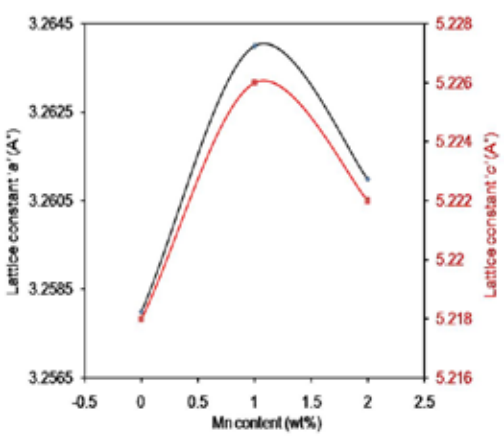


Figure 3 (a). Chemical composition profile of undoped ZnO nanoparticle.

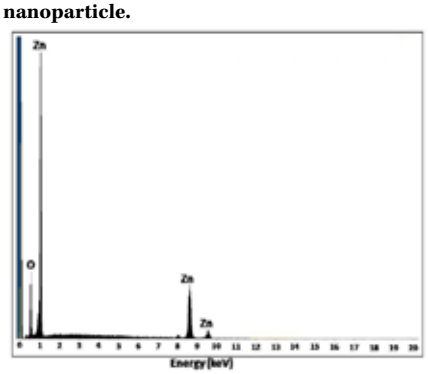


Figure 3(b). Chemical composition profile of Mn-1% sample.

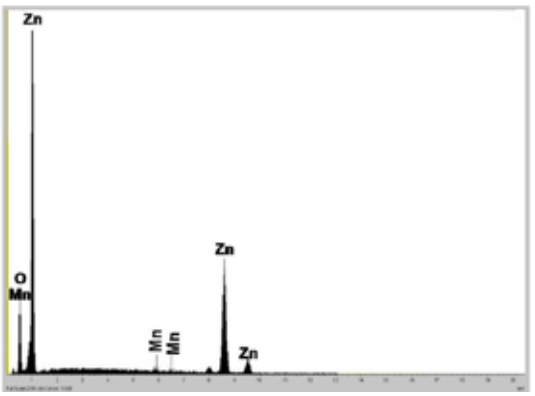


Figure 3(c). Chemical composition of 2% Mn doped ZnO nanoparticle.

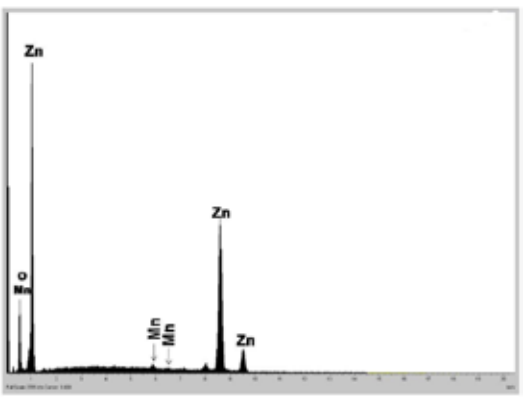


Figure 4 (a). SEM image of the undoped ZnO nanoparticle.

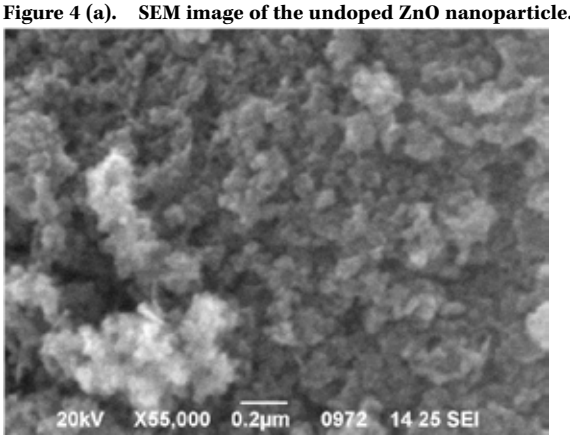
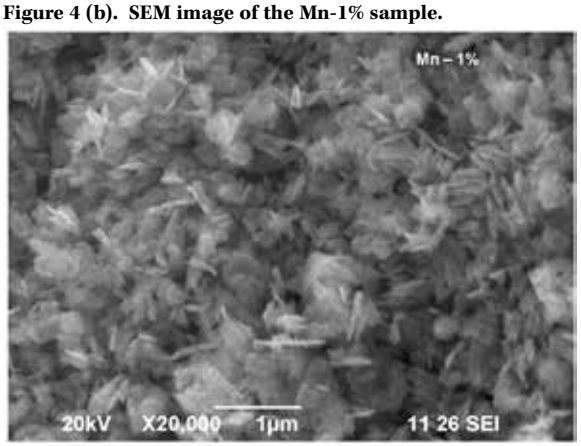


Figure 4 (b). SEM image of the Mn-1% sample.



Volume : 4 | Issue : 10 | October 2015 • ISSN No 2277 - 8179

Figure 4 (c). SEM image of the Mn-1% sample.

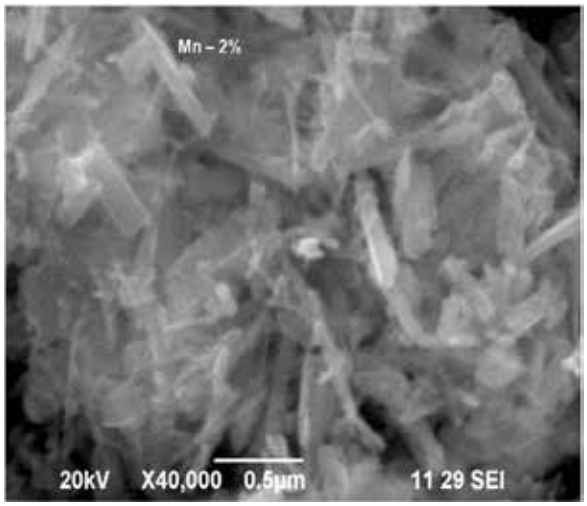


Figure 5(a). Energy gap of undoped ZnO nanoparticles. The graph has been drawn using the UV-Vis transmittance data.

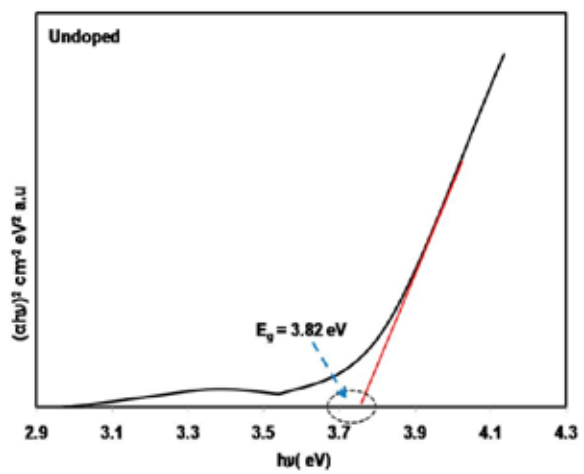


Figure 5(b). Energy gap of Mn-1% sample. The graph has been drawn using the UV-Vis transmittance data.

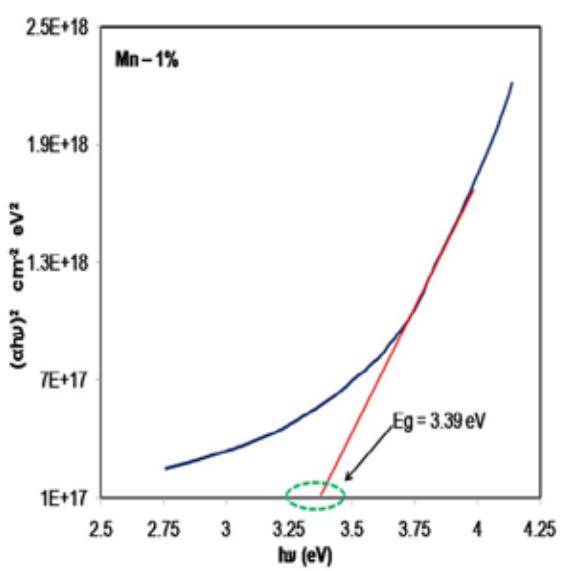


Figure 5(c). Energy gap of Mn-1% sample. The graph has been drawn using the UV-Vis transmittance data.

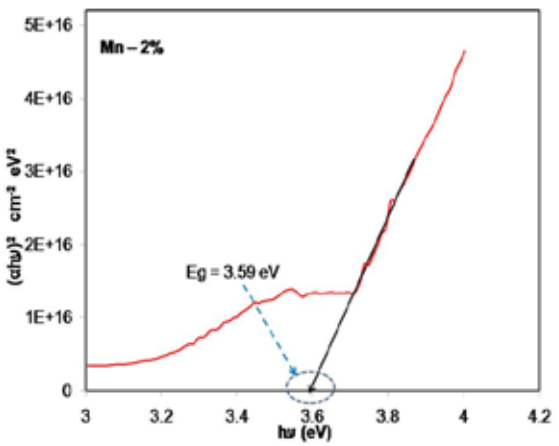


Figure 6(a). Room temperature Photoluminescence spectrum of undoped ZnO, displays near band edge and deep level emission bands

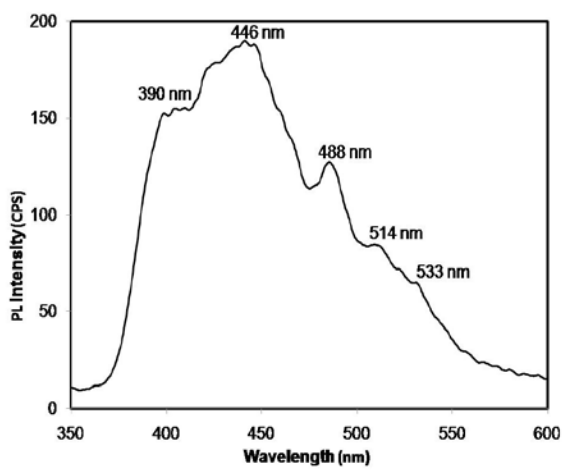


Figure 6(b). Photoluminescence spectrum of the 1% and 2% Mn doped samples

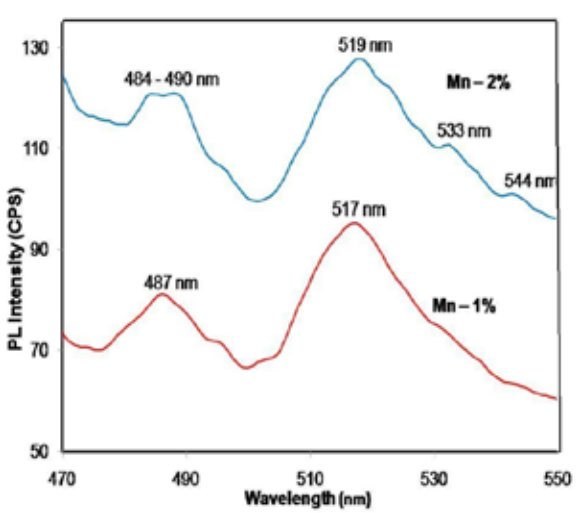
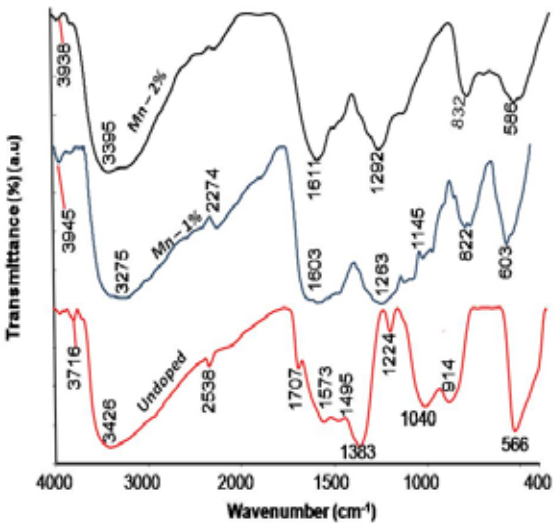


Figure 7. FTIR spectrum of the prepared samples. Spectrum of doped samples witnesses the incorporation of Mn ions in the site of Zn.



REFERENCE

1. L. Spanhel, M.A. Anderson, J. Am. Chem. Soc.113 (1991) 2826-2833. | | 2. E. A. Meulenkamp, J. Phys. Che. B 102 (1998) 5566-5572. | | 3. C.N.R. Rao, A. Müller, A.K. Cheetham, Mater. Manuf. Process. 23 (2008) 545-546. | | 4. K. Pushpanathan, S. Sathya, M. Jay Chithra, S. Gowthami, R. Santhi, Mater. Manuf. Process. 27 (2012) 1334-1342 | | 5. Seema Rani , Poonam Suri , P.K.Shishodia , R.M.Mehra, Solar Energy Mater. Solar Cells, 92 (2008) 1639–1645. | | 6. K.Nakahara, H.Takasu, P.Fons, A.Yamada, K.Matsubara, R.Hunger, S.Niki, Appl. Phys. Lett. 79 (2001) 4139–4141. | | 7. G. Zhou, J. Deng, Mater. Sci. Semicond. Process, 10 (2007) 90–96 | | 8. D.P. Norton, M.Ivill, Y.Li, Y.W. Kwon, J.M.Eric, H.S. Kim, K.Ip, S.J. Pearton, Y.W. Heo, S.Kim, B.S. Kang, F.Ren, A.F. Hebard, J.Kelly, Thin Solid films 496 (2006) 160-168. | | 9. Y. Li, J. Gong, Y. Deng, Sens. Actuators, A 158 (2010) 176-182. | | 10. C.Y. Luan, Y.K. Liu, Y. Jiang, J.S. Jie, I. Bello, S.T. Lee, J.A. Zapien, Vacuum 86 (2012) 737-741. | | 11. J. Sun, F.J. Liu, H.Q. Huang, J.W. Zhao, Z.F. Hu, X.Q. Zhang, Y.S. Wang, Appl. Surf. Sci. 257 (2010) 921-924. | | 12. A. Manavbasi, J.C. LaCombe, J. Lumin 128 (2008) 129-134. | | 13. V.R. Bandi, B.K. Grandhe, K.I. Kiwan Jang, H.S. Lee, D.S. Shin, S.S. Yi, J.H. Jeong, J. Alloys Compd. 512 (2012) 264-269. | | 14. S.Muthukumaran, R.Gopalakrishnan, J. Mater. Sci. - Mater. Electron, DOI 10. 1007/s 10854 -011-0604-6 | | 15. Sonal Singhal, Japinder Kaur, Tsering Namgyal, Rimi Sharma, Physica B: Phys. Condens. Matter 407 (2012) 1223-1226. | | 16. S. Suwanboon, P. Amornpitoksuk, Procedia Engineering 32 (2012) 821-826. | | 17. J. Nayak, S. Kimura, S. Nozaki, H. Ono, K. Uchida, Superlattices Microstruct. 42 (2007) 438-443. | | 18. Yu-Chih Tseng, Yow-Jon Lin, Hsing-Cheng Chang, Ya-Hui Chen, Chia-Jyi Liu, Yi-Yan Zou, J. Lumin, 132 (2012) 491-494. | | 19. J. El Ghoul, C. Barthou, L. El Mir, Superlattices Microstruct. 51 (2012) 942-951. | | 20. R. Varadhaseshan, S. Meenakshi Sundar, Appl. Surf. Sci. 258 (2012) 7161– 7165. | | 21. H. L. Yan, J. B. Wang, X. L. Zhong, Y. C. Zhou, Appl. Phys. Lett 93 (2008) 142592(1)-142592(3). | | 22. T. Dietl, H.Ohno, F. Matsukura, J.Cibert. D. Ferrand, Science 287 (2000) 1019-1022. | | 23. P. Sharma, A. Gupta, K. V. Rao, F. J. Owens, R. Sharma, R. Ahuja, J. M. O.Gillen, B. Johasson, G. A. Gehring, Nat. Mater 2 (2003) 673 - 677. | | 24. O.D. Jayakumar, H.G. Salunke, R.M, Kadam, M, Mohapatra, G, Yaswant, S.K. Kulshreshta, Nanotechnology 17 (2006) 1278–1285. | | 25. R.K. Zheng, H. Liu, X.X. Zhang, V.A.L. Roy and A.B.Djurisic: Appl. Phys. Lett 85 (2004) 2589-2594. | | 26. S.J. Han, T.H. Jang, Y.B. Kim, B.G. Park, J.H. Park and Y.H. Jeong: Appl. Phys. Lett., 83 (2003) 920-922. | | 27. C. Chen, B.Yu, P.Liu, J.F. Liu L.Wang, J. Ceramic Proc. Res. 12 (2011) 420-425. | | 28. N.Rajkumar, K.Ramachandran, Intern. J. Nanosci. 9 (2010) 495-502. | | 29. R. Ullah, J.Dutta, In Proceedings - 3rd International Conference on Emerging Technologies (ICET 2007) (2007) 306 – 311. | | 30. Cullity, B. D. Elements of X-ray diffraction, 2nd edition. (Addison- Wesley Publishing Co., Inc., Reading, MA, USA, 1978) p. 102 | | 31. S. Senthilkumaar, K. Rajendran, S. Banerjee, T.K. Chini, V. Sengodan , Mater. Sci. Semicond. Process. 11 (2008) 6-12. | | 32. A.K. Singh, J. Optoelect. Advan. Mater 12 (2010) 2255-2260. | | 33. M.E. Abrishami, S.M. Hosseimi, A. Kompany, J. Appl. Sci. 11 (2011) 1411-1415. | | 34. Nadia Febiana Djaja, Rosari Saleh, Mater.Sci.Appl. 3 (2012) 245-252. | | 35. K.F. Lin, H.M. Cheng, H.C. Hsu, L.J. Lin, W.F. Hsieh, Chem. Phys. Lett. 409 (2005) 208–211. | | 36. J.Anghel, A.Thurber, D.A. Tenne, C.B. Hanna, A. Punnose, J. Appl. Phys 107 (2010) 09E314 (1) - 09E3314 (3). | | 37. S. Deka, P.A.Joy, Solid State Commun. 142 (2007) 190–194. | | 38. M.Kitano, T. Hamabe, S. Maeda, T. Okabe, J. Cryst. Growth 128 (1993) 1099-1103. | | 39. Changchun Chena, Benhai Yua, Ping Liub, JiangFeng Liua, Lin Wang, J.Ceramic Proces. Res. 12 (2011) 420-425. | | 40. D.Sreekantha Reddy, S.K. Sharma, Y.D. Reddy, B.S.Reddy, K.R. Gunasekar, J Optoelectron. Adv. Mater. 10 (2008) 2607-2610 | | 41. Q. Qi, T. Zhang, S. Wang, X. Zhang, Sens. Actuators B: Chemical 137 (2009) 649-655. | 42. L. Yuan, B. Dierre, J. B. Wang, B. P. Zhang, T. Sekiguchi, J. Nanosci. Nanotech. 7 (2007) 3323-3327. | | 43. H. L. Yan, X. L. Zhong, J. B. Wang, G. J. Huang, S. L. Ding, G. C. Zhou, Y. C. Zhou, Appl. Phys. Lett. 90 (2007) 082503-082505. | | 44. H. L. Yan, J. B. Wang, X. L. Zhong, Y. C. Zhou, Appl. Phys. Lett. 93 (2008) 142592-142593. | | 45. J. Coates, Interpretation of Infrared Spectra, A Practical Approach, ed. by R.A. Meyers Encyclopedia of Analytical Chemistry (Wiley, Chichester, 2000), 10815. |